Comparison of 2-Dimensional and 3-Dimensional ^{82}Rb Myocardial Perfusion PET Imaging

Karin Knešaurek, PhD; Josef Machac, MD; Borys R. Krynyckyi, MD; and Orlandino D. Almeida, MD

Division of Nuclear Medicine, Mount Sinai Medical Center, New York, New York

We compared 2-dimensional (2D) and 3-dimensional (3D) ^{82}Rb PET imaging in 3 different experiments: in a realistic heart–thorax phantom, in a uniformity-resolution phantom, and in 14 healthy volunteers. **Methods:** A nonuniform heart–thorax phantom was filled with 111 MBq of ^{82}Rb injected into the left ventricular (LV) wall. In the LV wall of the cardiac phantom, 3 inserts—1, 2, and 3 cm in diameter—were placed to simulate infarcts. A standard rest cardiac PET imaging protocol in 2D and 3D modes was used. Following the same protocol, a uniformity-resolution phantom with uniformly distributed activity of 1,998 MBq and 740 MBq of ^{82}Rb in water was used to obtain 2D PET images and 3D PET images, respectively. All 2D volunteer studies were performed by injecting 2,220 MBq of ^{82}Rb intravenously. For half the volunteers, 3D studies were performed with a high dose (HD) (2,220 MBq) of ^{82}Rb; for the remainder of the 3D studies, a low dose (LD) (740 MBq) of ^{82}Rb was used. In the 2D and LD 3D studies, there was a delay of 2 min and 3 min, respectively, followed by a 6-min acquisition. In the HD 3D volunteer studies, there was a delay of 5 min followed by a 6-min acquisition. Circumferential profiles of the short-axis slices and the contrast of the inserts were used to evaluate the cardiac phantom PET images. The transaxial slices from the uniformity-resolution phantom were evaluated by visual inspection and by measuring uniformity. The human studies were evaluated by measuring the contrast between LV wall and LV cavity, using linear profiles and visual analysis. **Results:** In the cardiac phantom study, circumferential profiles for the 2D and 3D images were similar. The contrast values for the 1-, 2-, and 3-cm inserts in the 2D study were 0.19 ± 0.03, 0.34 ± 0.05, and 0.61 ± 0.03, respectively. The respective contrast values in the 3D study were 0.15 ± 0.02, 0.36 ± 0.04, and 0.52 ± 0.05. In the uniformity-resolution phantom study, the coefficients of variation, calculated for a representative uniform slice, were 5.3% and 7.6% for the 2D and 3D studies, respectively. For the 7 volunteers on whom HD 3D was used, the mean 2D contrast was 0.33 ± 0.08 and the mean HD 3D contrast was 0.35 ± 0.08 (P = not statistically significant). For the other 7 volunteers, on whom LD 3D was used, the mean 2D contrast was 0.39 ± 0.06 and the mean LD 3D contrast was 0.39 ± 0.10 (P = not statistically significant). In the tomographic slices, the 2D and 3D images and polar plots were similar. **Conclusion:** When obtained with a PET system having a high counting-rate performance, 2D and 3D ^{82}Rb PET cardiac images are comparable. LD 3D imaging can make ^{82}Rb PET cardiac imaging more affordable.

Key Words: 3-dimensional PET; 2-dimensional PET; ^{82}Rb; myocardial perfusion

J Nucl Med 2003; 44:1350–1356

Recently, 3-dimensional (3D)-mode PET imaging has gained considerable attention. It has been used mostly in brain studies (*1–3*) and, most recently, for tumor imaging (*4*). There is also interest in the use of 3D mode in myocardial perfusion ^{82}Rb PET imaging (*5–9*). Because of the short half-life of ^{82}Rb, cardiac images tend to be count poor. Although the 2-dimensional (2D) mode is expected to have slightly better axial resolution, the 3D mode is expected to have a higher sensitivity. However, the 3D mode suffers from high random events and scatter, including scatter from activity outside the field of view (FOV), from saturation problems because the PET camera is a paralyzable system, and from a highly nonuniform axial FOV (*10*). The counting rate performance characteristics of a PET system and the ratio of true, scatter, and random events in the total detected prompt events is expressed as a noise equivalent count (NEC) rate (*10*,*11*). The NEC rate increases as a function of activity concentration, measured in kBq/cm^3 (μCi/cm^3); reaches a peak; and declines as the system saturates at higher activity concentrations. A PET system with a high-counting-rate capability is essential for 3D imaging, because the system can easily become saturated with a high number of random and scatter events in addition to true events. For our system, DeGrado et al. (*11*) have shown that the peak NEC is greater in 2D than in 3D scanning for a uniform phantom. This finding may lead to the conclusion that 2D imaging performs better than 3D imaging. A possible explanation is that the higher number of "counts" in 3D imaging does not necessarily mean better image quality, because the increase in "counts" is mostly in scatter and random events. A recent comparison of 2D and 3D ^{82}Rb PET cardiac images on a different dedicated PET system (*12*) concluded that 2D images were superior. Because the Advance PET system (General Electric Medical Systems) has better counting rate performance (*10–14*), we wished to

Received Nov. 7, 2002; revision accepted Mar. 28, 2003.

For correspondence or reprints contact: Karin Knešaurek, PhD, Division of Nuclear Medicine, Box 1141, One Gustave L. Levy Place, New York, NY 10029.

E-mail: karin.knesaurek@mountsinai.org

determine whether similar or different results would ensue with this system.

MATERIALS AND METHODS

The same PET system was used for all acquisitions in both 2D and 3D modes. The system has 18 detector rings and 12,096 bismuth germanate 4 × 8 × 30 mm crystals. In the 2D mode, the system uses a tungsten collimator 1 × 120 mm in size. The axial FOV is 15.2 cm covered by 35 image planes. The axial sampling interval is 4.25 mm. The transaxial FOV is 55.0 cm. The coincidence window width is 12.5 ns, and the energy window is in the range of 300–650 keV. All 2D acquisitions were performed in high-sensitivity mode. The 2D images were reconstructed using a filtered backprojection reconstruction method and a Hanning smoothing filter with a 0.5 cycle/mm cutoff. Three-dimensional studies were reconstructed using an algorithm of Kinahan and Rogers (*15*). The matrix size was 128 × 128, and the pixel size was 4.29 mm. Attenuation correction using an 8-min transmission scan was applied in all studies. In the 2D studies, the scatter correction of Bergstrom et al. (*16*) was applied. For 3D data, scatter correction was performed by fitting the tails of the sinogram to a 2D gaussian distribution (*17*).

A nonuniform heart–thorax phantom (RH-2; Kyoto Scientific Specimen Co., Ltd.) was filled with 111 MBq (3 mCi) of ^{82}Rb injected into the left ventricular (LV) wall using our remote filling system (Fig. 1A). In the LV wall of the cardiac phantom, 3 inserts—1, 2, and 3 cm in diameter—were placed to simulate infarcts (Fig. 1B). A standard cardiac PET imaging protocol was used for the rest study, with the septa in (i.e., in 2D mode) and with the septa out (i.e., in 3D mode). For the cardiac phantom studies, emission and transmission scans were 8 min for both imaging modes. Corresponding short-axis slices (Figs. 2A and 2B) were used for comparison and analysis of the 2D and 3D data. In addition, circumferential profiles of the short-axis slices (Fig. 2C) and the contrast of the inserts were used to evaluate the cardiac phantom 2D and 3D PET images (Table 1). The contrast value was calculated as a ratio, C = (A − B)/(A + B), where A and B are the average activities in the hot and cold areas, respectively.

A uniformity-resolution deluxe phantom (Data Spectrum) was used to obtain 2D and 3D PET images. The volume of the phantom with the inserts is 6.0 L. For both 2D and 3D studies, the emission scan was 10 min and the transmission scan was 8 min. For the 2D study, the phantom was filled with a uniformly distributed 1,998 MBq (54 mCi) of ^{82}Rb and water, and in the 3D study, an activity of 740 MBq (20 mCi) of ^{82}Rb was used.

The levels of radioactivity for imaging the phantoms were selected on the basis of our choosing a counting rate of less than 2,000 kcps for 2D and 3D PET acquisitions. This 2,000-kcps counting rate was empirically selected because, on our PET system, below this threshold the number of true counts was higher than the number of random counts, resulting in reconstructed images of good quality. In 2D phantom studies with applied activities, the threshold was never reached. However, for the 3D uniformity-resolution phantom study with an activity of 740 MBq, the start of acquisition needed to be delayed until the counting rate fell below 2,000 kcps.

The transaxial slices from the uniformity-resolution phantom (Fig. 3) were evaluated by visual inspection and by measuring image noise for uniformity sectors of the phantom. Second-row, third-column images in Figures 3A and 3B are representative

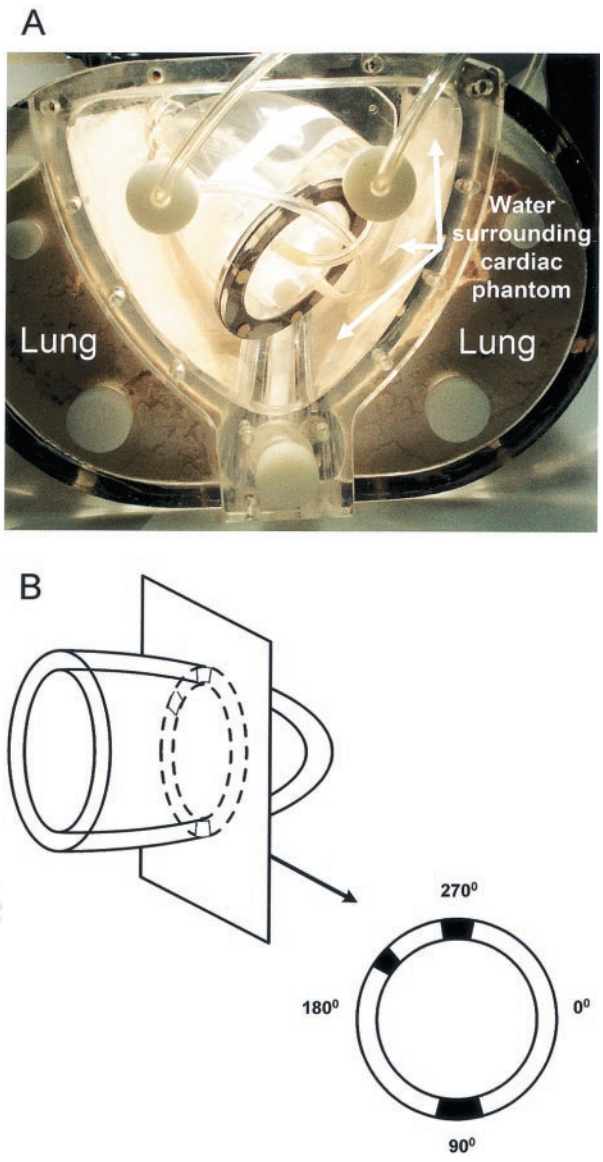

FIGURE 1. (A) RH-2 heart–thorax phantom. Teflon (Dupont) rod simulates spine, and sawdust simulates lungs. Cardiac phantom is placed in water. LV wall is connected by flexible plastic tubing to remote filling system. (B) In LV wall, 3 inserts—1, 2, and 3 cm in diameter—were placed in same short-axis plane. Three-centimeter insert was placed at 90°, 1-cm insert at 200°, and 2-cm insert at 270°.

uniformity sectors for noise calculations. Image noise was defined as the coefficient of variation (COV, 100 × SD/mean [%]).

The phantom studies were performed to help us understand how to optimally acquire and process 2D and 3D ^{82}Rb myocardial studies on our PET system. The results of the phantom studies, in addition to providing necessary experience, gave us a guideline on how to proceed with the volunteer studies. Seven male and 7 female healthy human volunteers participated in our study. None of the volunteers had a history of cardiac disease. Written informed consent was obtained from each volunteer. The human protocol was approved by the Institutional Review Board of our Medical Center. All volunteer 2D studies were performed by injecting 2,220 MBq (60 mCi) of ^{82}Rb intravenously. For half the volun-

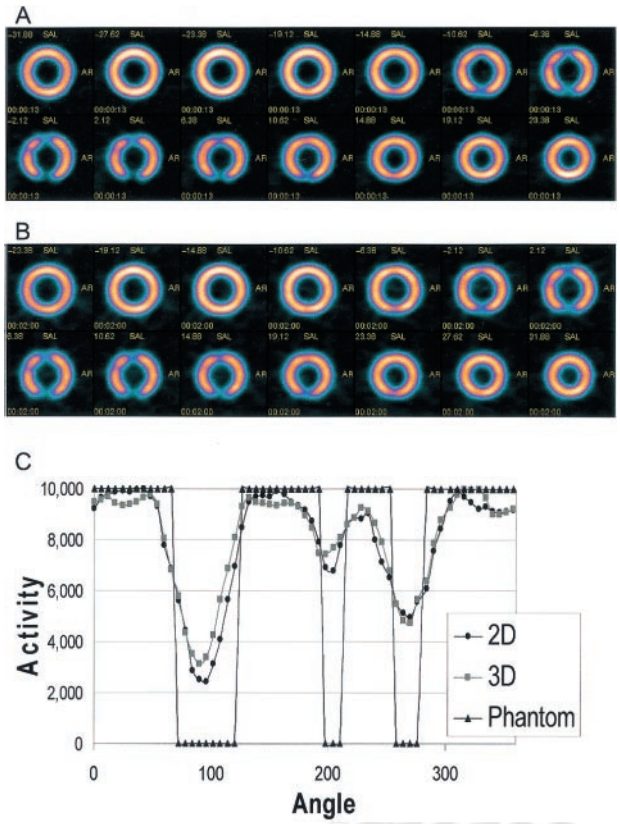

FIGURE 2. Short-axis slices from 2D cardiac phantom ^{82}Rb study (A) and short-axis slices from 3D cardiac phantom ^{82}Rb study (B). (C) Circumferential profiles from short-axis slices shown in A and B.

teers, 3D studies were performed with a high dose (HD) (2,220 MBq [60 mCi]) of ^{82}Rb; for the reminder of the 3D studies, a low dose (LD) (740 MBq [20 mCi]) of ^{82}Rb was used. In the 2D studies and LD 3D studies, there was a delay of 2 min and 3 min, respectively, from the time of injection, followed by a 6-min acquisition. In the HD 3D volunteer studies, there was a delay of 5 min followed by a 6-min acquisition. Blood-pool activity and the ratio of random versus true counts determined the delay. Attenuation correction was performed using an 8-min transmission scan in both 2D and 3D clinical studies. All studies were performed while the volunteers were at rest. The clinical studies were evaluated by linear profiles in the transaxial slices (Fig. 4); by the contrast between the LV wall and LV cavity; and by visual inspection of the horizontal long-axis, vertical long-axis, and short-axis slices and of polar plots.

RESULTS

Figures 2A and 2B show the 2D and 3D cardiac phantom data, respectively. All 3 inserts are visible in the short-axis slices. Comparing visually the 2D and 3D cardiac phantom data, one can conclude that they are similar. Circumferential profiles from the short-axis slices shown in Figures 2A and 2B, normalized to the same maximum value, are given in Figure 2C. The true phantom profile is shown for comparison. The contrast values for the 1-, 2-, and 3-cm inserts in the 2D and 3D studies are given in Table 1. Three adjacent slices on which all 3 inserts were seen the best were used to calculate contrast values. The results showed that 2D images had slightly better contrast for the 1-cm and 3-cm insert; for the 2-cm insert, contrast was similar.

Two-dimensional and 3D images from the uniformity-resolution phantom are shown in Figure 3. In both the 2D and the 3D transaxial slices, all 5 cold spheres were clearly visible. In the cold rod area, 2 segments were clearly visible, that is, the areas of the rods that were 12.7 and 11.1 mm in diameter. The COV values for 2D and 3D data were calculated from the circular region of interest covering uniform hot areas shown in the second-row, third-column images of Figures 3A and 3B, respectively. Our results showed the 2D COV to be 5.3% and the 3D COV to be 7.6%. Thus, the 3D study was a little noisier.

The total number of counts (true, scatter, and random events) in the 2D phantom study was 11,708.7 kilocounts, and the number of random events was 4,669.2 kilocounts; that is, randoms constituted 39.9% of the total counts. In the 3D study, the total number of counts was 20,355.1 kilocounts. The number of random events was 9,101.4 kilocounts; that is, randoms constituted 44.7% of the total counts.

For each of the 14 healthy volunteers, the contrast values between the LV wall and LV cavity for the same 2D and 3D slices are given in Table 2. For the 7 volunteers who underwent an HD 3D study, the mean 2D contrast was 0.33 ± 0.08 and the mean HD 3D contrast was 0.35 ± 0.08. The paired *t* test analysis gave a *P* value of 0.37 (not statistically significant). For the other 7 volunteers, who underwent LD 3D studies, the mean 2D contrast was 0.39 ± 0.06 and the mean LD 3D contrast was 0.39 ± 0.10. The paired *t* test analysis gave a *P* value of 0.90 (not statistically significant). The analysis showed that the values of the mean contrast in 2D and 3D studies were very close, regardless of whether a high or low 3D dose was used.

The first volunteer, subject 1 in Table 2, was a relatively lightweight (63 kg) 48-y-old, 177-cm-tall man. Figures 4A and 4B show, respectively, clinical 2D and HD 3D ^{82}Rb PET images of transaxial heart slices. The profiles for 2D and HD 3D ^{82}Rb cardiac studies, normalized to the same maximum values, along the line shown in Figure 4A are shown in Figure 4C. The contrast between LV wall and LV

TABLE 1
Comparison of Contrast Values for 2D and 3D PET in Cardiac Phantom Study

Type of PET	Contrast value		
	1-cm insert	2-cm insert	3-cm insert
2D	0.19 ± 0.03	0.34 ± 0.05	0.61 ± 0.03
3D	0.15 ± 0.02	0.36 ± 0.04	0.52 ± 0.05

Contrast was calculated as (maximum − minimum)/(maximum + minimum). Data are mean ± SD.

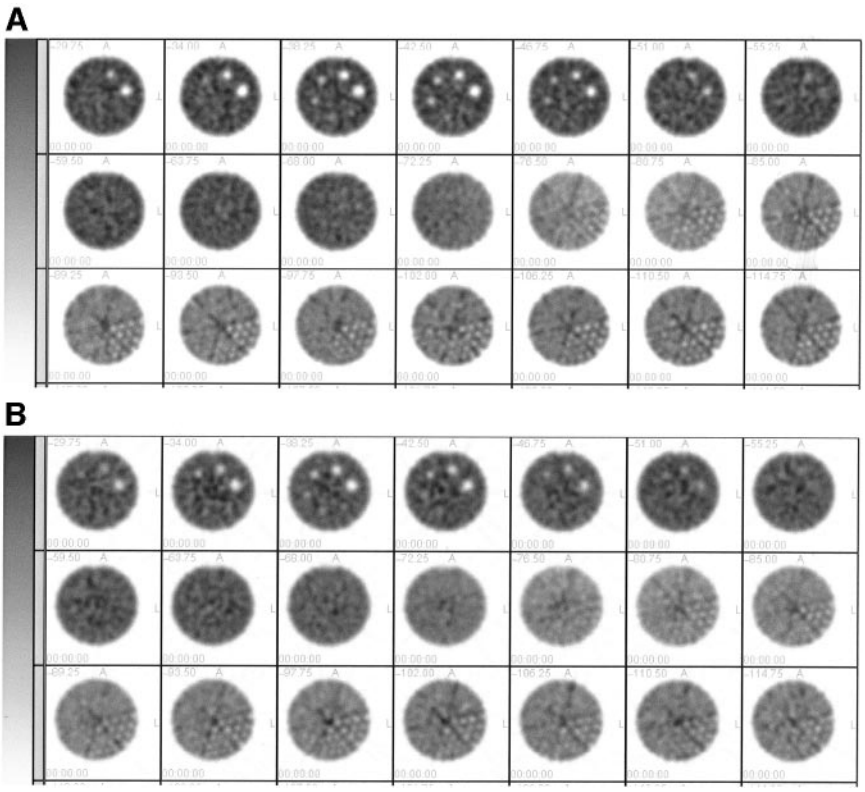

FIGURE 3. Transaxial slices from uniformity-resolution phantom ^{82}Rb study: 2D images (A) and 3D images (B).

cavity (Table 2) was 0.29 for 2D data and 0.27 for HD 3D data. The reconstructed images are shown in Figure 5. The images are similar in quality, that is, in contrast, noise level, and scatter from adjunct activity. The same comparison was repeated on a larger volunteer. Figure 6 shows the results for a 54-y-old, 183-cm, 90-kg man. Again, in the 3D study, the higher dose of ^{82}Rb was used. The 2D and 3D images are similar. Figure 7 compares the 2D and 3D PET images when the lower dose of ^{82}Rb was used in the 3D study. The subject is a 75-kg, 188-cm, 32-y-old man. The 2D and 3D images are comparable.

DISCUSSION

In all 3 experiments, that is, cardiac phantom, uniformity-resolution phantom, and clinical studies, the 2D and 3D images were comparable. In the cardiac phantom experiment, the 3D PET images had a higher fraction of scatter and random events in the total counts, causing slightly higher background than in the 2D images. Our results indicated that this increase in background, compared with that in the 2D images, was minimized when the delay between the time of injection and the start of acquisition was appropriately prolonged. In our uniformity-resolution phantom experiment, by waiting until the counting rate dropped below 2,000 kcps, we achieved a fraction of randoms in the total counts very close between 3D and 2D imaging, that is, 44.7% and 39.9%, respectively. Circumferential profiles in the cardiac phantom experiment and linear profiles in the volunteer experiments, both normalized to the same maxi-

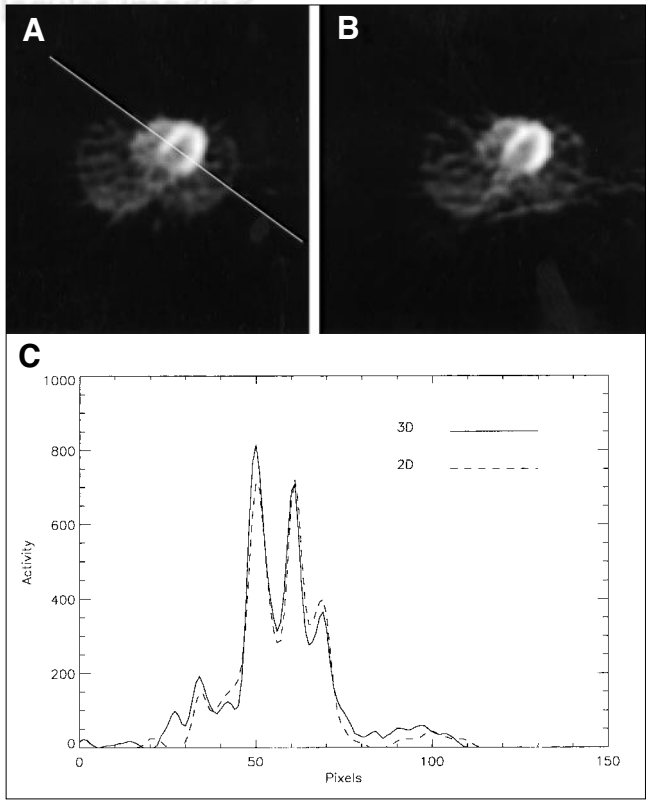

FIGURE 4. Transaxial slices from clinical ^{82}Rb study on volunteer: 2D image (A) and HD 3D image (B). (C) Profiles of 2D and 3D volunteer data along line shown in A.

TABLE 2
Comparison of Contrast Values for 2D and 3D PET in Cardiac Human Studies

Subject no.	Contrast value	
	2D PET	3D PET
1	0.29	0.27
2	0.41	0.41
3	0.38	0.36
4	0.42	0.41
5	0.20	0.22
6	0.30	0.35
7	0.34	0.41
Mean ± SD	0.33 ± 0.08	0.35 ± 0.08
8	0.39	0.39
9	0.45	0.45
10	0.28	0.26
11	0.46	0.56
12	0.40	0.32
13	0.38	0.42
14	0.40	0.34
Mean ± SD	0.39 ± 0.06	0.39 ± 0.10

Contrast was calculated as (maximum − minimum)/(maximum + minimum). Subjects 1–7 underwent HD 3D PET; subjects 8–14 underwent LD 3D PET. *P* (by paired *t* test) = 0.37 for 2D PET vs. HD 3D PET and 0.90 for 2D PET vs. LD 3D PET.

mum counts, were very similar in the 3D and 2D studies, as was measured contrast. The comparison of 2D and 3D (HD and LD) studies indicated that clinical images in patients of moderate weight (less than 80 kg) were also very close. The results of phantom and clinical studies strongly indicated that on a PET system having a high counting-rate performance, one can obtain 2D and 3D ^{82}Rb PET images of comparable quality.

Our first clinical protocol specified activity of 2,220 MBq (60 mCi) in 2D and 3D ^{82}Rb PET myocardial studies, with 2-min and 5-min delays in 2D and 3D studies, respectively. The delay of 2 min in the 2D mode is needed for blood-pool clearance. One would at first expect HD 3D images to be of higher quality than 2D images, because of the increased number of counts in HD 3D imaging. However, high-activity 3D-mode imaging results in higher randoms and scatter fraction, and there is a saturation point. Consequently, the HD 3D studies did not provide better images than the 2D studies because of the 5-min acquisition delay needed to reduce the high randoms rate and total counting rate as required to maintain adequate image quality. This offsets the increase in sensitivity for HD 3D imaging. Thus, one can obtain similar results in 3D mode from a lower dose, allowing acquisition to begin earlier. In volunteer 3D studies for which we used the lower activity, a 3-min delay was used because the initial counting rate was not as high as in HD 3D studies. Because of the higher sensitivity of 3D-mode imaging, it has the advantage of having the same counting rate as the HD 2D mode but with a lower injected dose. This could lead to significant cost savings in the purchase of an ^{82}Rb generator and make myocardial ^{82}Rb PET imaging more affordable.

Further work is needed on finding optimal acquisition and processing parameters for ^{82}Rb PET myocardial imaging in 3D mode. Preliminary data show that the noise level obtained in 3D studies is comparable to the noise level in 2D studies. We speculate that a combination of several factors, including blood-pool clearance, a high level of scatter and random counts, timing of acquisition, the 75-s ^{82}Rb half-life, and patient size (*18*), plays a significant role in the determination of optimal acquisition and processing parameters for 3D ^{82}Rb PET myocardial imaging. A high level of scatter and random counts, that is, the high level of noise as a function of injected dose, can be addressed by a NEC study in a similar manner to one recently performed for ^{18}F whole-body PET imaging (*19*). The NEC analysis is a necessary step to investigate the influence of random and scatter counts, and counting properties of the system, as a function of activity used. However, the NEC analysis does not provide all the information needed for protocol optimization, particularly in ^{82}Rb PET myocardial imaging, be-

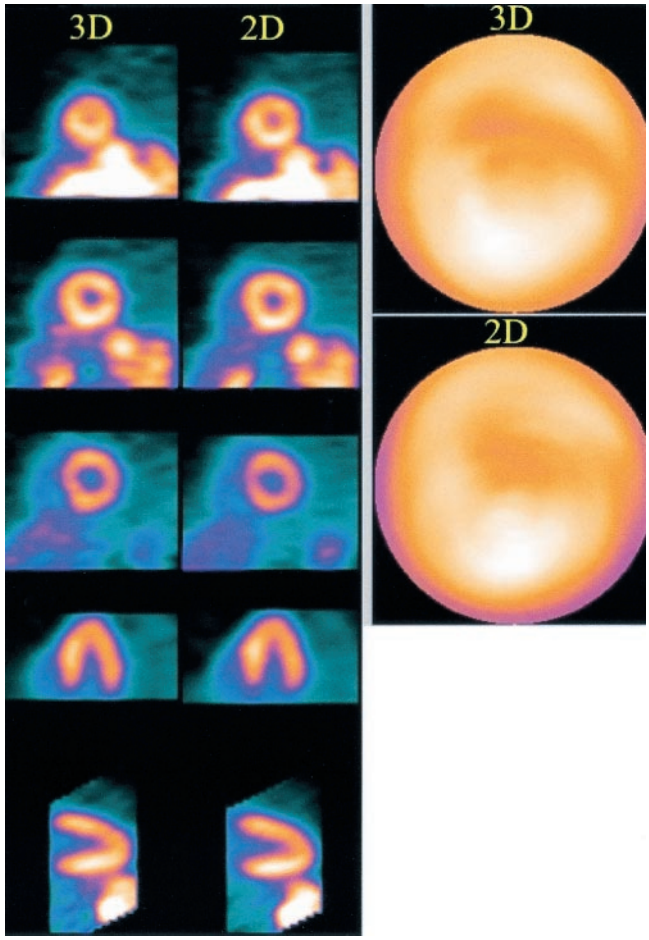

FIGURE 5. Results of comparison for light (63 kg, 177 cm) volunteer, for HD 3D and 2D studies. Subject is same as in Figure 4.

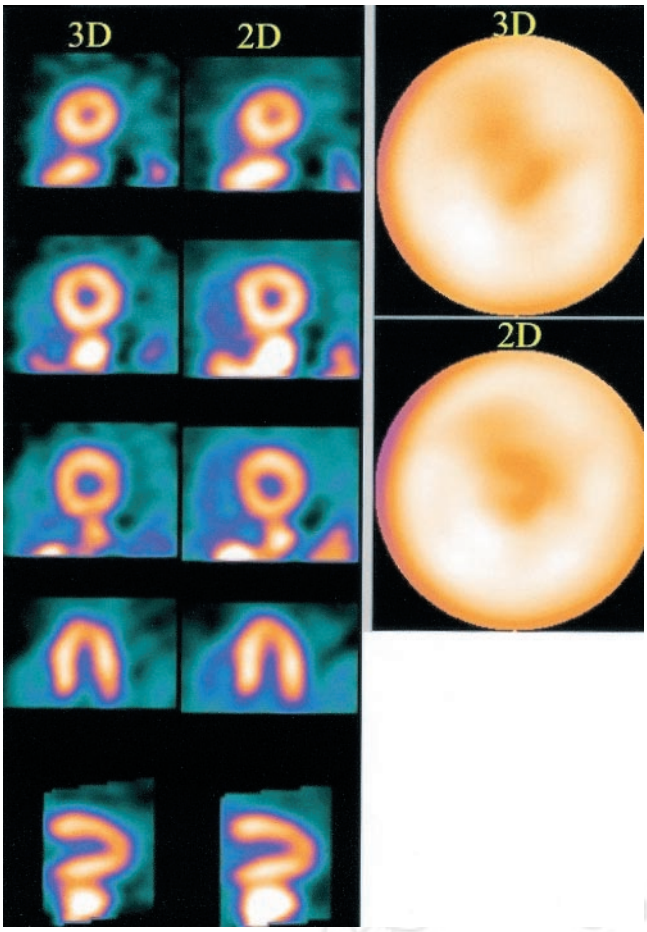

FIGURE 6. Results of comparison for heavier (90 kg, 183 cm) volunteer, for HD 3D and 2D studies.

cause of rapidly changing blood-pool activity and the very short ^{82}Rb half-life.

At present, our routine myocardial ^{82}Rb PET perfusion studies are done in 2D mode. Three-dimensional studies require significantly more acquisition and processing time and disk space. Performing several 3D studies saturates the storage capacity of our computer system quickly. However, 3D myocardial ^{82}Rb PET perfusion imaging is feasible on a PET system having a high counting-rate performance. With further development, the 3D mode may become routine. The full potential of 3D PET imaging will be achieved by applying more accurate randoms and scatter corrections (*20*), by using faster and better electronics, by reducing the coincidence time window and improving counting characteristics, by using optimal crystal detectors, and by improving reconstruction software and computer hardware (*21*).

CONCLUSION

Optimization of acquisition and processing parameters for ^{82}Rb PET myocardial imaging in the 2D and 3D modes is a demanding task. It depends on the scanner counting rate performance, usually described by NEC, and ^{82}Rb kinetics in a patient's body, which are influenced by the short ^{82}Rb half-life, blood-pool clearance, and the patient's size. Relatively rapid ^{82}Rb decay requires injection of a high activity to avoid count-poor clinical images. However, initial activity is limited by the scanner counting rate performance, that is, paralyzation; a high rate of random; and, to a lesser extent, scatter events at a high counting rate. Balancing these 2 mutually opposite activity requirements is even more hampered by the required delay between injection of ^{82}Rb and the start of myocardium imaging, because of blood-pool clearance. This balance between the counting rate limitations of PET systems and the desire for high-count clinical images is more difficult in 3D-mode PET imaging than in 2D mode because of the higher rate of random and scatter events. However, 3D mode has appeal because of the higher sensitivity and the possibility of using lower doses. In ^{82}Rb PET myocardial imaging, it is of special interest to determine whether and when LD 3D ^{82}Rb PET myocardial imaging can replace more expensive 2D or HD 3D ^{82}Rb PET myocardial imaging. Clinical use of LD 3D ^{82}Rb PET myocardial imaging could potentially reduce the tracer costs and make ^{82}Rb PET myocardial imaging more affordable. This study represents a step forward in resolving this important issue by comparing 2D and 3D

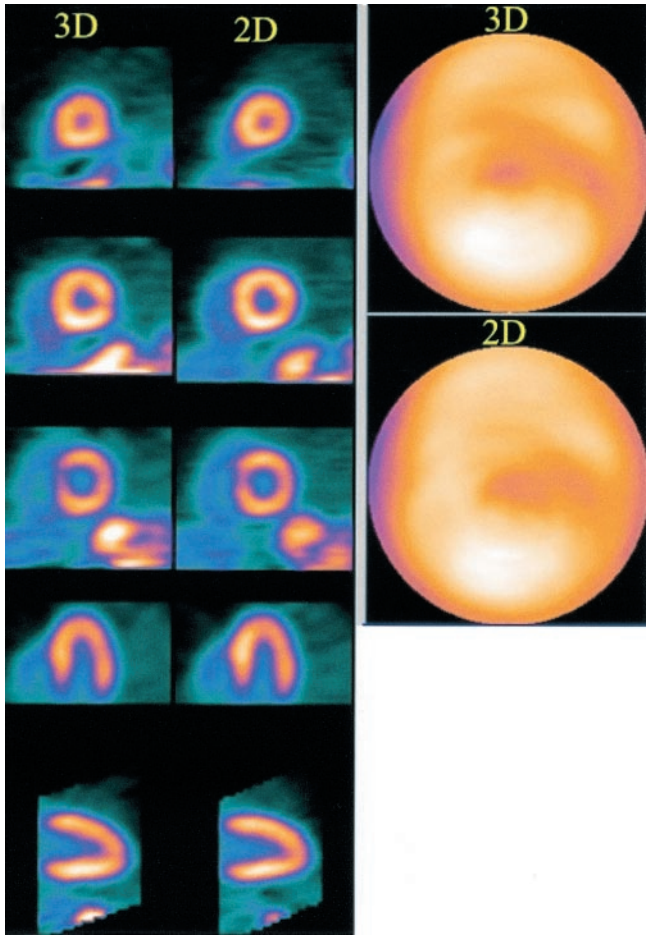

FIGURE 7. Results of comparison for normal-weight (75 kg, 188 cm) volunteer, for LD 3D and 2D studies.

^{82}Rb PET myocardial imaging on a PET system having a high counting-rate performance. Our results are slightly different from the results presented in the recent similar comparison between 2D and 3D ^{82}Rb PET myocardial imaging (*12*). This is not a contradiction, because of the differences attributed to the PET systems used. We believe that our PET system has adequate counting rate performance and can provide images of relatively good counts in both 2D and 3D modes. Further improvement of the characteristics of the PET system will lead to better and more affordable ^{82}Rb PET myocardial imaging and will influence the choice of the preferable clinical mode, that is, 2D versus 3D. However, presently, the results of this study suggest that on a PET system having a high counting-rate performance, 2D and 3D myocardial ^{82}Rb perfusion studies provide images of comparable quality.

REFERENCES

1. Cherry SR, Woods RP, Hoffman EJ, Mazziota JC. Improved detection of focal cerebral blood flow changes using three-dimensional positron emission tomography. *J Cereb Blood Flow Metab.* 1993;13:630–638.
2. Sadato N, Carson RE, Daube-Whiterspoon ME, Campbell G, Hallett M, Herscovitch P. Optimization of noninvasive activation studies with ^{15}O-water and three-dimensional positron emission tomography. *J Cereb Blood Flow Metab.* 1997;17:732–739.
3. Moreno-Cantu JJ, Thompson CJ, Zatorre RJ. Evaluation of the ECAT EXACT HR+ 3-D PET scanner in $H_2{}^{15}O$ brain activation studies: dose fractionation strategies for rCBF and signal enhancing protocols. *IEEE Trans Med Imaging.* 1998;17:979–985.
4. Kalff V, Hick RJ, Ware RE, et al. The clinical impact of ^{18}F-FDG PET in patients with suspected or confirmed recurrence of colorectal cancer: a prospective study. *J Nucl Med.* 2002;43:492–499.
5. Mullani NA, Goldstein RA, Gould KL, et al. Myocardial perfusion with rubidium-82. I. Measurement of extraction fraction and flow with external detectors. *J Nucl Med.* 1983;24:898–906.
6. Goldstein RA, Mullani NA, Marani SK, Fisher DJ, Gould KL, O'Brien HA Jr. Myocardial perfusion with rubidium-82. II. Effects of metabolic and pharmacologic interventions. *J Nucl Med.* 1983;24:907–915.
7. Goldstein RA, Mullani NA, Wong WH, et al. Positron imaging of myocardial infarction with rubidium-82. *J Nucl Med.* 1986;27:1824–1829.
8. Yoshida K, Mullani N, Gould KL. Coronary flow and flow reserve by PET simplified for clinical applications using rubidium-82 or nitrogen-13-ammonia. *J Nucl Med.* 1996;37:1701–1712.
9. Lin JW, Robert R. Sciacca RR, Chou R-L, Laine AF, Bergmann SR. Quantification of myocardial perfusion in human subjects using Rb-82 and wavelet-based noise reduction. *J Nucl Med.* 2001;42:201–208.
10. Pajevic S, Daube-Witherspoon ME, Bacharach SL, Carson RE. Noise characteristics of 3D and 2D PET images. *IEEE Trans Med Imaging.* 1998;17:9–23.
11. DeGrado TR, Turkington TG, Williams JJ, Stearns CW, Hoffman JM, Coleman RE. Performance characteristics of a whole-body PET scanner. *J Nucl Med.* 1994;35:1398–1406.
12. Votaw JR, White M. Comparison of 2D and 3D cardiac Rb-82 PET studies. *J Nucl Med.* 2001;42:701–706.
13. Weinhard K, Eriksson L, Grootoonk S, Casey M, Pietrzyk U, Heiss WD. Performance evaluation of the positron scanner ECAT EXACT. *J Comput Assist Tomogr.* 1992;16:804–813.
14. Lewellen TK, Kohlmyer RS, Miyaoka RS, Kaplan MS. Investigation of the performance of the General Electric ADVANCE positron emission tomograph in 3D mode. *IEEE Trans Nucl Sci.* 1996;NS-43:2199–2206.
15. Kinahan PE, Rogers JG. Analytic three dimensional image reconstruction using all detected events. *IEEE Trans Nucl Sci.* 1989;NS-36:964–968.
16. Bergstrom M, Eriksson L, Bohm C, Blomqvist G, Litton J. Correction for scatter radiation in a ring detector positron camera by integral transformation of the projections. *J Comput Assist Tomogr.* 1983;10:845–850.
17. Stearns CW. Scatter correction method for 3-D PET using 2-D fitted gaussian functions [abstract]. *J Nucl Med.* 1995;36(suppl):105P.
18. Kadrmas DJ, Christian PE, Wollenweber SD, Kohlmyer SG, Stearns CW. Comparative evaluation of 2D and 3D lesion detectability on a full-ring BGO PET scanner [abstract]. *J Nucl Med.* 2002;43(suppl):57P.
19. Lartizien C, Comtat C, Kinahan PE, et al. Optimization of the injected dose based on noise equivalent count rates for 2- and 3-dimensional whole-body PET. *J Nucl Med.* 2002;43:1268–1278.
20. Ollinger JM. Model-based scatter correction for fully 3D PET. *Phys Med Biol.* 1996;41:153–176.
21. Knešaurek K. New developments in PET instrumentation: quo vadis PET? *J Nucl Med.* 2001;42:1831–1832.